J Mater Sci: Mater Electron (2017) 28:8423–8428
DOI 10.1007/s10854-017-6560-z

Zinc oxide nanoparticles: solvent-free synthesis, characterization and application as heterogeneous nanocatalyst for photodegradation of dye from aqueous phase

Mojgan Goudarzi[1] · Mehdi Mousavi-Kamazani[1] · Masoud Salavati-Niasari[2]

Received: 25 December 2016 / Accepted: 7 February 2017 / Published online: 24 February 2017

Abstract In present study, for the first time, ZnO nanoparticles have been synthesized via a simple, novel, solvent and template free solid-state thermal decomposition of the mixed $Zn(NO_3)\cdot 6H_2O$ and cochineal powders as a novel starting reagent at 600 °C for 3 h. The as-prepared product was analyzed by XRD, EDS, SEM, TEM, FT-IR and DRS. Besides, the effect of cochineal powder on the morphology and particle size of ZnO nanoparticles was investigated. The results exhibited that cochineal powder prevents the sintering of nanoparticles and leads to formation of uniform particles. Moreover, the efficiency of ZnO nanoparticles as a photocatalyst for the decolorization of methylene orange (MO) has been evaluated and 90% degradation of MO was obtained after 120 min.

1 Introduction

Much attention has been paid to zinc oxide (ZnO) nanostructures since they have unique features such as optical transparency, electric conductivity, piezoelectricity and near-UV emission [1, 2] and play important roles in different branches of science, such as chemical sensors [3], catalysts [4], UV light-emitters [5], photovoltaics [6], cantilevers [7], photocatalyst for photocatalytic degradation of water pollutants [8] and other optoelectronic devices [9]. So, considerable efforts and various methods have been reported to synthesize of this metal oxide nanostructures such as co-precipitation [8], hydrothermal [10], thermal evaporation [11], chemical vapor method (CVD) [12], pulsed laser deposition (PLD) [13], microemulsion [14], solvothermal [2], sonochemical [15] and solid-state thermal decomposition [16]. Among them, thermal decomposition is a novel, suitable and useful method to produce stable monodispersed nanoparticles and it is much cleaner and economical [17–19]. However, an improvement in thermal decomposition process should be made in preparing ZnO nanoparticles with controllable size and shape because in all cases which have been reported in literatures by this method a suitable solvent such as oleylamine, oleic acid and ethylene glycol and a suitable precursor such as [N,N-bis(salicylaldehydo) ethylene diamine]zinc(II) and bis(acetylacetonato)zinc(II) is needed [17–19]. For example Choi et al. [20] reported a method for the large-scale synthesis of uniform-sized hexagonal pyramid-shaped ZnO nanocrystals by the thermolysis of Zn–oleate complex. Salavati-Niasari et al. [21] have synthesized uniform ZnO nanoparticles by thermal decomposition of zinc acetylacetonate in oleylamine. And so, monodisperse ZnO nanoparticles were successfully prepared through the decomposition of zinc acetylacetonate precursor [22]. Kanade et al. [23] have investigated the effect of particle size of ZnO synthesized via thermal decomposition of zinc oxalate at 450 °C. Muruganandham and Wu [24] have reported synthesis of ZnO nanobundles from zinc oxalate by decomposition at 400 °C for 12 h. In this work, we present a solvent and precursor-free approach for preparation of ZnO nanoparticles by simple solid-state thermal decomposition of mixed zinc nitrate and cochineal powders at 600 °C. In the solid-state approach, all of the biological components of the cochineal including carminic acid molecules and proteins are taking

✉ Masoud Salavati-Niasari
salavati@kashanu.ac.ir

[1] Young Researchers and Elites Club, Arak Branch, Islamic Azad University, Arak, Iran

[2] Institute of Nano Science and Nano Technology, University of Kashan, Kashan, P. O. Box. 87317-51167, Islamic Republic of Iran

part in the reaction and their high steric hindrance prevent from agglomeration of the as-formed nuclei [25]. Finally, the obtained ZnO nanoparticles were utilized as a photocatalyst for decolorization of methylene orange (MO) was evaluated.

2 Experimental

2.1 Materials and characterization

All the chemicals reagents were of analytical grade and were used as received without further purification. Cochineal powder was obtained from the dried bodies of female scale insects species, *Dactylopius coccus*, which feed on wild cacti. X-ray diffraction (XRD) patterns were recorded by a Philips-X'PertPro, X-ray diffractometer using Ni-filtered Cu Kα radiation at scan range of $10 < 2\theta < 80$. The energy dispersive spectrometry (EDS) analysis was studied by XL30, Philips microscope. Scanning electron microscopy (SEM) images were obtained on LEO-1455VP equipped with an energy dispersive X-ray spectroscopy. Transmission electron microscopy (TEM) images were obtained on a Philips EM208 transmission electron microscope with an accelerating voltage of 100 kV. Optical analyses were performed using a V-670 UV–Vis–NIR Spectrophotometer (Jasco). GC-2550TG (Teif Gostar Faraz Company, Iran) were used for all chemical analyses. FTIR spectrums were obtained on Magna-IR, spectrometer 550 Nicolet with 0.125 cm^{-1} resolution in KBr pellets in the range of 400–4000 cm^{-1}.

2.2 Synthesis ZnO nanoparticles

The starting powders (0.3 g of $Zn(NO_3)\cdot 6H_2O$ and 0.5 g of cochineal) was milled and mixed in a ball mill for 20 min using zirconia grinding media. Then, the powder mixtures were calcined at 600 °C for 3 h. Finally, it was washed with distilled water and ethanol several times and dried at 50 °C for 10 h (sample A). To investigate the effect of cochineal powder a blank test were carried out without cochineal (sample B).

2.3 Photocatalysis experiments

In order to evaluate photocatalytic activity of the ZnO, photocatalytic degradation of methylene orange (MO) dye was under taken. A typical experiment constitutes ZnO nanoparticles (20 mg) were added into a glass beaker containing of 150 mL of aqueous dye solution (5 mg/L in ethanol as solvent), and then dispersed by stirring for 30 min at 20–25 °C in darkness to establish adsorption–desorption equilibrium between the dye molecules and ZnO surface. Later, a series of UV lamps (6 × 15 W, Philips) were switched on a 20 cm distance over the suspension surface. Finally, the absorbance of dye solution at its maximum absorption wavelength (510 nm for MO) was recorded by a UV–Vis spectrophotometer (Shimadzu UV–Vis spectrometer) and the decolorization rate was calculated according to the absorbance change. The decolorization efficiency (%) is calculated as Eq. 1.

$$(\%) = (A_0 - A)/A_0 \times 100 \quad (1)$$

where A_0 is the initial absorption of dye and A is the absorption of dye after photo irradiation.

3 Results and discussion

Crystalline structure and phase purity of as-prepared product has been determined using XRD. The XRD pattern of as-prepared ZnO nanoparticles in the presence of cochineal powder (sample A) is shown in Fig. 1. The diffraction peaks observed in Fig. 1 can be indexed to pure hexagonal phase of zinc oxide (a = b = 3.2539 Å, c = 5.2098) with space group of P63mc and JCPDS No. 80-0075. No diffraction peaks from other species could be detected, which indicates the obtained sample is pure. The crystallite diameter (D_c) of ZnO nanoparticles estimated by the Scherrer formula shown in Eq. 2 [26] is 18 nm.

$$D_c = K\lambda/\beta\cos\theta \quad (2)$$

where β is the breadth of the observed diffraction line at its half intensity maximum, K is the so-called shape factor, which usually takes a value of about 0.9, and λ is the wavelength of X-ray source used in XRD. Chemical purity of product (sample A) was examined by energy dispersive X-ray spectroscopy (EDX) (Fig. 2), which indicates only

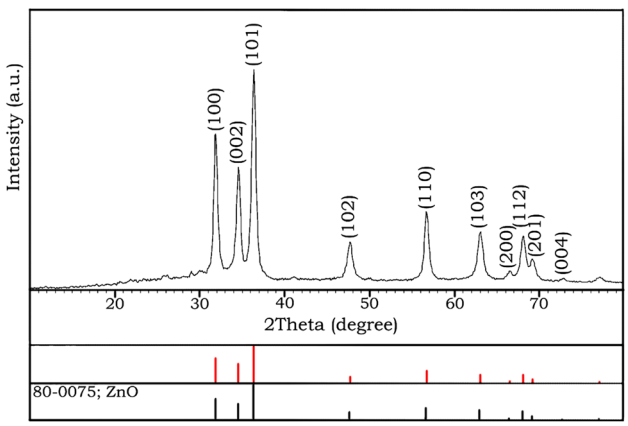

Fig. 1 XRD pattern of the as-synthesized ZnO nanoparticles

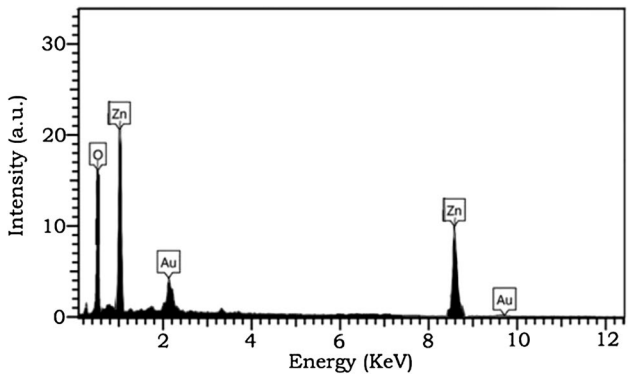

Fig. 2 EDX spectrum of the as-synthesized ZnO nanoparticles

Zn and O peaks exist in the sample except the peak due to the use of a Au-coated substrate for sample examination. In addition, neither N nor C signals were detected in the EDS spectrum. Therefore, both XRD and EDX analyses show that pure ZnO nanoparticles are successfully produced via the mentioned synthetic route. Different scales of SEM images were taken in order to characterize the morphology, size, and microstructure of the products (Fig. 3). From SEM images (Fig. 3a, b) it can be seen that the morphology of the as-synthesized ZnO in the presence of cochineal powder (sample A) is the spherical nanoparticles with average particle size ~15–25 nm that aggregated together at some points. However, when the same reaction was performed in the absence of cochineal powder (sample B), agglomerated microstructures were obtained (Fig. 3c, d). As a result, cochineal powder prevents the sintering of nanoparticles and leads to formation of uniform particles. To assess the size and morphology of as-prepared zinc oxide nanoparticles (sample A), transmission electron microscopy (TEM) analysis was performed. The TEM image of the zinc oxide nanoparticles as-prepared in present cochineal showed in (Fig. 4). The TEM image of the zinc oxide demonstrate that nanoparticles with spherical morphology are uniform and arranged. Furthermore, the image illustrate that as-prepared nanoparticles have size in the range of 15–25 nm, with the emphasis on the SEM image in Fig. 3.

It has been reported that the band gap (Eg) has a main impact on the determining the nanostructured materials characteristics utilized in photocatalytic applications and is oftentimes calculated from the UV–Vis diffuse reflectance data [27]. Figure 5a, b show the UV–Vis diffuse reflectance

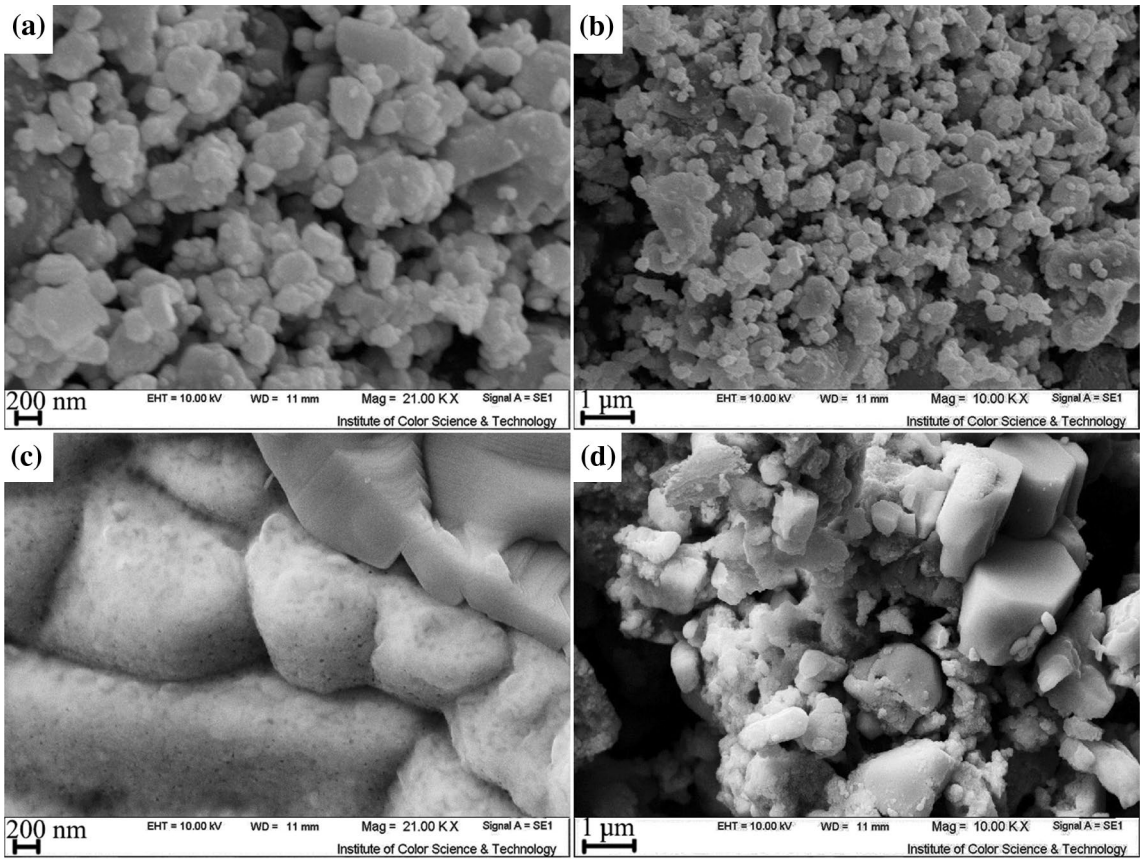

Fig. 3 Different scales of SEM images of the as-synthesized ZnO (**a, b**) in the presence cochineal and (**c, d**) without cochineal

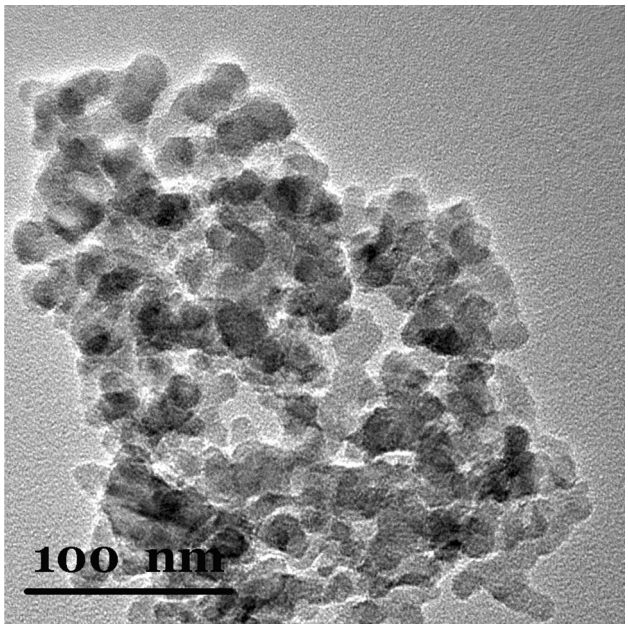

Fig. 4 TEM image of the as-synthesized ZnO nanoparticles

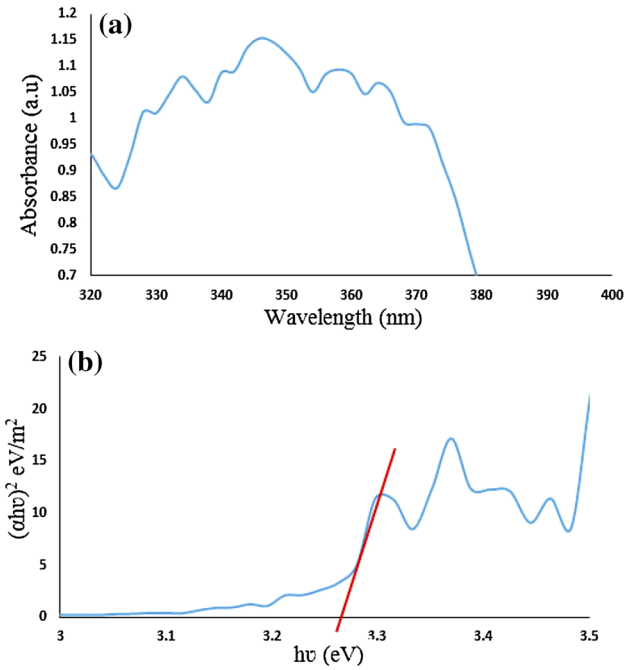

Fig. 5 UV–Vis diffuse reflectance spectrum (**a**) and plot to determine the band gap (**b**) of as-synthesized ZnO nanoparticles (sample A)

spectroscopy of as-synthesized ZnO nanoparticle in the presence of cochineal powder (sample A). The fundamental absorption edge in most semiconductors follows the exponential law. Using the absorption data, the band gap was estimated by Tauc's relationship:

$$\alpha = \frac{\alpha_0(h\upsilon - E_g)^n}{h\upsilon}$$

where α is absorption coefficient, hν is the photon energy, α0 and h are the constants, Eg is the optical band gap of the material, and n depends on the type of electronic transition and can be any value between 1/2 and 2 [28]. The energy gap of the as-synthesized ZnO has been determined by extrapolating the linear portion of the plots of $(\alpha h\upsilon)^{22}$ against (hυ) to the energy axis (Fig. 5b). The Eg value is calculated 3.27 eV for the as-synthesized ZnO nanoparticles.

Figure 6a, b show the FTIR spectra of the mixture before and after calcination, respectively. As can be seen (Fig. 6a), a significant peak at ~3349 cm^{-1} is attributed to the γ(OH) stretching [29]. Moreover, the bands at 2923 and 2853 cm^{-1} are related to C–H stretching and the two peaks at 1652 and 1044 cm^{-1} could be attributed to C=O and C–C bonds [30–32]. Furthermore, the absorption peak at 1382 cm^{-1} corresponds to –COOH symmetry stretching vibrations, while the band at 599 cm^{-1} confirms the presence Zn–O bind [30–32]. The FT-IR spectrum of the calcined product (sample A) is illustrated in Fig. 6b. According to Fig. 6b, it is obvious that after calcination and washing with ethanol and water there are no important peaks indicating that there is not any organic molecule (from cochineal) absorbed on the surface of the as-synthesized ZnO nanoparticles. Two peaks at 3439 and 458 cm^{-1} could be attributed to O–H and Zn–O bonds, respectively.

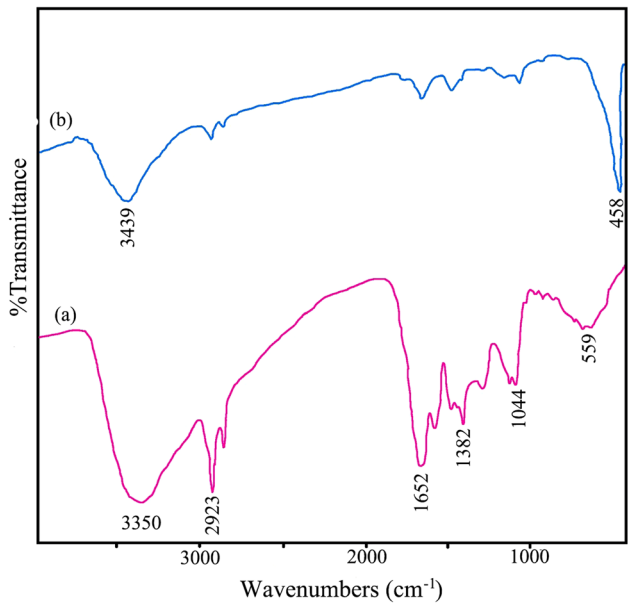

Fig. 6 FT-IR spectra of sample A (*a*) before calcination and (*b*) after calcination at 600 °C

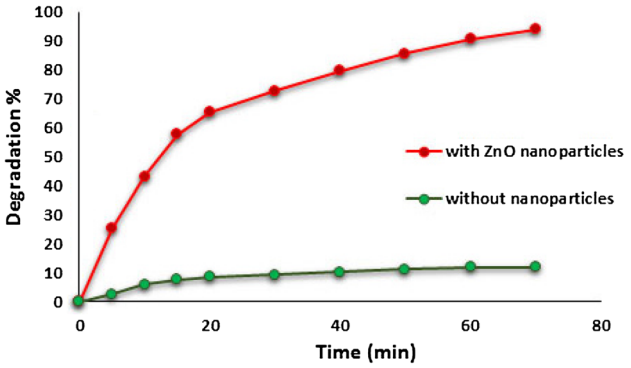

Fig. 7 Photodecolorization of MO under UV illumination by blank and ZnO nanoparticles (sample A)

To evaluate the photocatalytic decomposition of MO, the as-synthesized ZnO nanoparticles were used as photocatalyst. Moreover, the photocatalytic decomposition was done under UV-light illumination, and the degradation rate for the decomposition of MO was estimated by observing the changes in absorbance (absorption intensity vs. irradiation time) obtained by UV–Vis spectra. Figure 7 shows the plot of the degradation versus time intervals for the photocatalytic reaction of ZnO nanoparticles (sample A) and blank sample (without ZnO). According to Fig. 7, in absence of ZnO nanoparticles, almost negligible radiation of MO is observable while in the presence of ZnO more than 90% of MO was decolorized after 120 min.

In comparison with other similar works for synthesizing ZnO by thermal decomposition [17–24], our method is facile and low-cost. In accordance with our knowledge in all reports, the suitable solvent and precursor were used, but our method does not require any solvent and precursor. In our previous work [25, 33], we showed that natural dyes such as cochineal and pomegranate peel due to the appropriate molecules such as carminic acid and polyphenolic substances in their compounds can prevent the sintering of particles at high temperature. High temperatures lead to increase in particles growth and fusion and as a consequence, agglomeration of particles will occur [25].

4 Conclusion

In summary, ZnO nanoparticles with average particle size ~20 nm have been successfully prepared via facile and novel solid-state thermal decomposition of the mixed $Zn(NO_3)\cdot 6H_2O$ and cochineal powders at 600 °C for 3 h. The XRD and SEM results exhibited that cochineal powder prevents the sintering of nanoparticles. Moreover, ZnO nanoparticles were utilized as photocatalyst for the decolorization of MO under UV-light irradiation. The synthesized ZnO nanoparticles exhibited appreciable photocatalytic activity and in presence of ZnO, 90% degradation of MO was obtained after 120 min. The present strategy for the preparation of ZnO nanoparticles involves many advantages as it is a controllable, free solvent, template-less, and economical method.

Acknowledgements Authors are grateful to the council of Iran National Science Foundation (INSF) and University of Kashan for supporting this work by Grant No (159271/5279).

References

1. T. Kawano, H. Imai, Cryst. Growth Des. **6**, 1054 (2006)
2. M. Salavati-Niasari, F. Davar, A. Khansari, J. Alloys Compd. **509**, 61 (2011)
3. J. Tamaki, Sensor Lett. 3, 89 (2005)
4. M. Kurtz, J. Strunk, O. Hinrichsen, M. Muhler, K. Fink, B. Meyer, C. Wöll, Angew. Chem. Int. Ed. **44**, 2790 (2005)
5. C. Yang, J. Wang, W. Ge, L. Guo, S. Yang, D. Shen, J. Appl. Phys. **90**, 4489 (2001)
6. M. Izaki, K.-T. Mizuno, T. Shinagawa, M. Inaba, A. Tasaka, J. Electrochem. Soc. **153**, C668 (2006)
7. S.H. Lee, S.S. Lee, J.-J. Choi, J. Jeon, K. Ro, Microsyst. Technol. **11**, 416 (2005)
8. K. Vignesh, A. Suganthi, M. Rajarajan, S. Sara, Powder Technol. **224**, 331 (2012)
9. L. Vayssieres, K. Keis, S.-E. Lindquist, A. Hagfeldt, J. Phys. Chem. B **105**, 3350 (2001)
10. Q. Li, Y. Chen, L. Luo, L. Wang, Y. Yu, L. Zhai, J. Alloys Compd. **560**, 156 (2013)
11. S. Muthukumar, C. Gorla, N. Emanetoglu, S. Liang, Y. Lu, J. Cryst. Growth **225**, 197 (2001)
12. Y. Zhang, R.E. Russo, S.S. Mao, Appl. Phys. Lett. **87**, 043106 (2005)
13. T. You, J. Yan, Z. Zhang, J. Li, J. Tian, J. Yun, W. Zhao, Mater. Lett. **66**, 246 (2012)
14. J.Y. Liang, L. Guo, H.B. Xu, L. Jing, L.X. Dong, W.Z. Hua, W.Z. Yu, J. Weber, J. Cryst. Growth **252**, 226 (2003)
15. D. Qian, J. Jiang, P.L. Hansen, Chem. Commun. **3**, 1078 (2003)
16. J.C. Lin, B.-R. Huang, T.C. Lin, Appl. Surf. Sci. **289**, 384 (2014)
17. M. Salavati-Niasari, N. Mir, F. Davar, J. Alloys Compd. **476**, 908 (2009)
18. F. Soofivand, M. Salavati-Niasari, F. Mohandes, Mater. Lett. **98**, 55 (2013)
19. L. Wang, C. Ma, X. Ru, Z. Guo, D. Wu, S. Zhang, G. Yu, Y. Hu, J. Wang, J. Alloys Compd. **647**, 57 (2015)
20. S.H. Choi, E.G. Kim, J. Park, K. An, N. Lee, S.C. Kim, T. Hyeon, J. Phys. Chem. B **109**, 14792 (2005)
21. M. Salavati-Niasari, F. Davar, M. Mazaheri, Mater. Lett. **62**, 1890 (2008)
22. J. Liu, Y. Bei, H. Wu, D. Shen, J. Gong, X. Li, Y. Wang, N. Jiang, J. Jiang, Mater. Lett. **61**, 2837 (2007)
23. K. Kanade, B. Kale, R. Aiyer, B. Das, Mater. Res. Bull. **41**, 590 (2006)
24. M. Muruganandham, J. Wu, Appl. Catal. B **80**, 32 (2008)
25. M. Goudarzi, N. Mir, M. Mousavi-Kamazani, S. Bagheri, M. Salavati-Niasari, Sci. Rep. **6**, 32539 (2016)
26. M. Mousavi-Kamazani, M. Salavati-Niasari, M. Ramezani, J. Clust. Sci. **24**, 927 (2013)
27. M. Goudarzi, D. Ghanbari, M. Salavati-Niasari, J. Mater. Sci. Mater. Electron. **26**, 8798 (2015).

28. J. Tauc, R. Grigorovici, A. Vancu, Phys. Status Solidi B **15**, 627 (1966)
29. M. Mousavi-Kamazani, M. Salavati-Niasari, S.M. Hosseinpour-Mashkani, M. Goudarzi, Mater. Lett. **145**, 99 (2015)
30. M. Mousavi-Kamazani, M. Salavati-Niasari, M. Sadeghinia, Mater. Lett. **142**, 145 (2015)
31. M. Panahi-Kalamuei, S. Alizadeh, M. Mousavi-Kamazani, M. Salavati-Niasari, J. Ind. Eng. Chem. **21**, 1301–1305 (2015)
32. M. Salavati-Niasari, S. Alizadeh, M. Mousavi-Kamazani, N. Mir, O. Rezaei, E. Ahmadi, J. Clust. Sci. **24**, 1181–1191 (2013)
33. M. Goudarzi, Z. Zarghami, M. Salavati-Niasari, J. Mater. Sci. Mater. Electron. **27**, 9789 (2016).